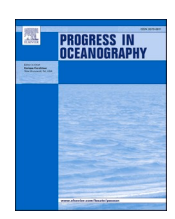
ELSEVIER

Contents lists available at ScienceDirect

# Progress in Oceanography

journal homepage: www.elsevier.com/locate/pocean



# Overflow water pathways in the North Atlantic

M. Susan Lozier <sup>a,\*</sup>, Amy S. Bower <sup>b</sup>, Heather H. Furey <sup>b</sup>, Kimberley L. Drouin <sup>c</sup>, Xiaobiao Xu <sup>d</sup>, Sijia Zou <sup>b,e</sup>

- <sup>a</sup> School of Earth and Atmospheric Sciences, Georgia Institute of Technology, Atlanta, GA 30318, United States
- b Department of Physical Oceanography, Woods Hole Oceanographic Institution, Woods Hole, MA 02543, United States
- <sup>c</sup> Nicholas School of the Environment, Duke University, Durham, NC 22710, United States
- <sup>d</sup> Center for Ocean-Atmosphere Prediction Studies, Florida State University, Tallahassee, FL 32310, United States
- e State Key Laboratory of Marine Environmental Science & College of Ocean and Earth Sciences, Xiamen University, Xiamen, China

#### ABSTRACT

As part of the international Overturning in the Subpolar North Atlantic Program (OSNAP), 135 acoustically-tracked deep floats were deployed to track the spreading pathways of Iceland-Scotland Overflow Water (ISOW) and Denmark Strait Overflow Water (DSOW) from 2014 to 2018. These water masses, which originate in the Nordic Seas, are transported by the deepest branch of the Atlantic Meridional Overturning Circulation (AMOC). The OSNAP floats provide the first directly-observed, comprehensive Lagrangian view of ISOW and DSOW spreading pathways throughout the subpolar North Atlantic. The collection of OSNAP float trajectories, complemented by model simulations, reveals that their pathways are (a) not restricted to western boundary currents, and (b) remarkably different from each other in character. The spread of DSOW from the Irminger Sea is primarily via the swift deep boundary currents of the Irminger and Labrador Seas, whereas the spread of ISOW out of the Iceland Basin is slower and along multiple export pathways. The characterization of these Overflow Water pathways has important implications for our understanding of the AMOC and its variability. Finally, reconstructions of AMOC variability from proxy data, involving either the strength of boundary currents and/or the property variability of deep waters, should account for the myriad pathways of DSOW and ISOW, but particularly so for the latter.

## 1. Introduction

Some of the earliest meridional hydrographic transects of the Atlantic, occupied nearly a century ago, revealed cold and fresh water at depth in the mid- and tropical latitudes that contrasted sharply with the overlying warm and salty thermocline waters (Warren, 1981; Richardson, 2008). Over the ensuing decades, the origin of these deep and abyssal waters was traced to surface waters at high latitudes in the northern and southern hemispheres using signatures of salinity and dissolved oxygen. These property signatures illustrate the meridional spread of the deep-water masses associated with the large-scale overturning circulation, commonly referred to as the global ocean conveyor belt in the latter part of the twentieth century (Broecker, 1991).

This two-dimensional view gained a third dimension with theoretical work in the 1950s and 1960s (Stommel, 1958; Stommel and Arons, 1959) that placed the equatorward spreading of abyssal waters at the western boundaries of the basins and restricted all poleward flow to the interior. In confirmation of this theory, waters sourced from the Nordic Seas that enter the North Atlantic over the sills of the Greenland-Scotland Ridge, as well as deep waters produced in the subpolar North Atlantic, were identified in hydrographic sections of the Deep Western

Boundary Current at downstream locations in the North Atlantic (e.g., Pickart, 1992; Doney and Jenkins, 1994; Smethie et al., 2000; Fischer et al., 2010; Toole et al., 2017).

When concerns arose in the early part of this century that the 'conveyor belt' was susceptible to rapid changes that would have severe climatic consequences, the desire to quantify changes in this circulation gave way to a definition that again collapsed the overturning to two dimensions (Wunsch, 2005). The Meridional Overturning Circulation (MOC), defined in terms of the zonally-integrated volume flux, supplanted the 'conveyor belt' as the term of reference for this circulation feature. Though the latter term is admittedly more descriptive, it was deemed too ambiguous for quantitative assessments of the MOC mean state and variability.

The upper limb of the Atlantic MOC, or AMOC, carries warm and salty waters poleward, where air-sea fluxes of heat and fresh water transform them into colder, fresher and denser waters carried equatorward in the lower limb. Because the deep, dense waters were understood to transit meridionally along the western boundaries of the basin, this collapse to two dimensions did not, at the time, seem particularly problematic.

Over the past two decades, there has been a strong focus on AMOC

<sup>\*</sup> Corresponding author at: Georgia Tech College of Sciences, Office of the Dean, 225 North Ave., Atlanta, GA 30332-0365, United States. E-mail address: susan.lozier@gatech.edu (M. Susan Lozier).

variability both in the observational and modeling domains (Srokosz et al., 2021). In parallel, a growing number of observational and modeling studies have shown that the equatorward spread of deep waters transported by the AMOC lower limb is not restricted to the confines of the deep western boundary currents (Lavender et al., 2000; Bower et al., 2009; Gary et al., 2012; Lozier et al., 2013; Biló and Johns, 2019). An intersection of these two study arcs has been somewhat rare, driven in part by the two-dimensionality of the AMOC definition and in part by the still-incomplete understanding of deep ocean current pathways.

We contend, however, that a fully-three-dimensional view of the spreading pathways of the deep waters carried by the AMOC lower limb is essential to a complete understanding of AMOC variability for several reasons. First, pathway definitions allow for an assessment of the time lag between changes in deep-water production and the downstream impact of these changes (Zhang, 2010; Yeager and Danabasoglu, 2014; Desbruyères et al., 2019). Second, the interpretation of deep-water mass properties at downstream locations requires an understanding of mixing along their pathways, which depends strongly on the length of those pathways (McCartney, 1992; Lozier, 1999; Smethie et al., 2000). Third, AMOC variability has been attributed to the advection and/or propagation of deep-water mass anomalies along the western boundaries of the North Atlantic (Delworth et al., 1993; Biastoch et al., 2008; Zhang, 2010; Polo et al., 2014; Yeager and Danabasoglu, 2014). An understanding of the upstream source of those anomalies, and the extent to which they are related to deep-water production changes, will aid the development of a mechanistic interpretation of AMOC variability. Finally, observed pathways serve as ground-truth for simulated water mass spreading in ocean and climate models. This ground-truthing is important since simulated AMOC variability is a function of which water masses, and in what volume, are exported from their source regions (Li and Lozier, 2018). Thus, in addition to making progress on the decadeslong quest to map the deep ocean circulation, we are motivated to understand the pathways of the AMOC lower limb to aid the interpretation of the observed AMOC variability.

A recent study based on Lagrangian observations and simulations provided a comprehensive review of the understanding to date of the pathways of the upper and lower AMOC limbs throughout the Atlantic (Bower et al., 2019). As described in that work, observational studies of lower limb AMOC pathways over the past 25 years have largely focused on the shallowest water in that limb, referred to as Upper North Atlantic Deep Water (UNADW). In comparison, Lagrangian observations of the pathways for the deepest waters in the lower limb, referred to as Lower North Atlantic Deep Water (LNADW), have been decidedly sparse. LNADW is principally sourced from dense Nordic Sea waters that flow southward across the sills of the Greenland-Scotland Ridge into the North Atlantic. These waters of Nordic Sea origin are collectively termed Overflow Waters (OW). Most of our inferences regarding OW spreading pathways in the North Atlantic have been gleaned from analyses of water property measurements gathered over the past few decades (e.g., McCartney, 1992; Dickson and Brown, 1994; Doney and Jenkins, 1994; Smethie et al., 2000; Daniault et al., 2016).

To provide a more complete picture for deep ocean pathways, the Overturning in the Subpolar North Atlantic Program (OSNAP; Lozier et al., 2017), initiated in 2014 to provide a trans-basin observing system for the continuous measure of the AMOC in the subpolar North Atlantic, also included multiple deployments of acoustically-tracked subsurface floats. Specifically, floats were launched into Iceland Scotland Overflow Water (ISOW) and Denmark Strait Overflow Water (DSOW) downstream of their respective entries into the subpolar North Atlantic (Fig. 1). Floats were also deployed in Northeast Atlantic Deep Water (NEADW) in the Irminger basin, a water mass that shares the same density range as ISOW but is sufficiently removed from ISOW's entry into the North Atlantic to justify a separate label, as explained in the following sections and as is consistent with several past studies (Swift, 1984; Dickson et al., 1994; Lazier et al., 2002). [Note: For the purpose of this paper, we refer to these three water masses collectively as 'OW' since NEADW shares the same density class as ISOW and is a modification of ISOW due to mixing with other water masses in the basin, such as Labrador Sea Water (LSW) and DSOW (Racapé et al., 2019).]

The 135 floats deployed as part of this program allow for the first comprehensive, observationally-based description of the pathways of these deep-water masses in the subpolar North Atlantic. That description

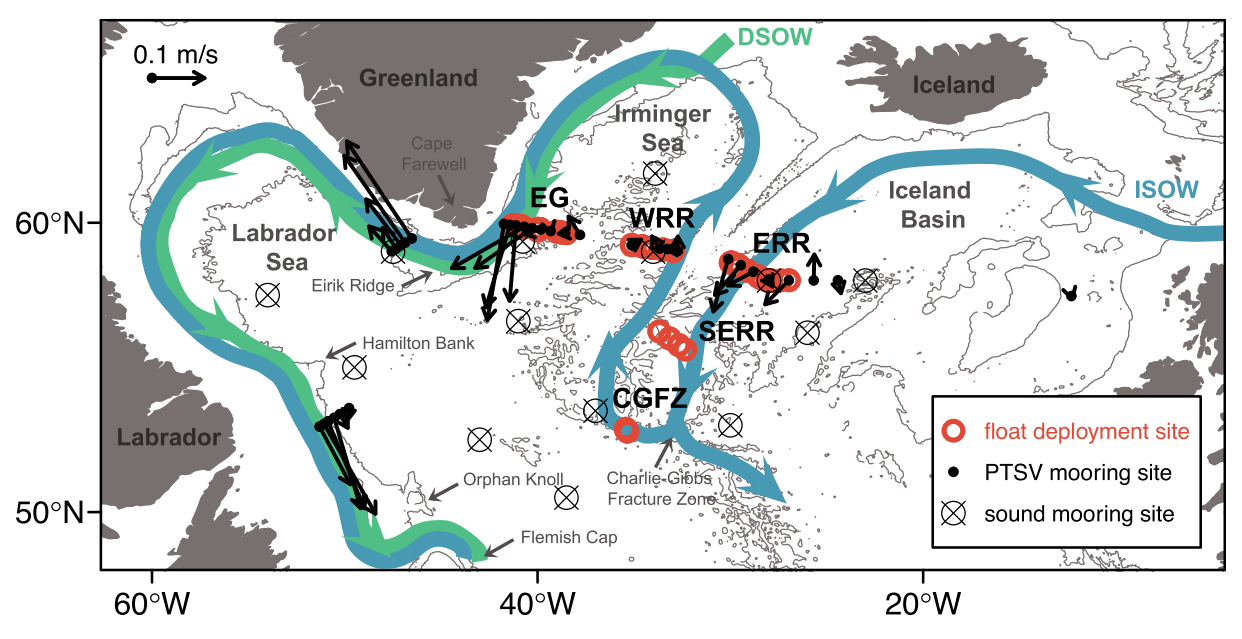


Fig. 1. Schematic of ISOW (blue line) and DSOW (green line) pathways, as generally understood prior to the beginning of the OSNAP program in 2014. OSNAP RAFOS float deployment sites (red open circles) and mooring sites (black circles) are marked. Black arrows at each OSNAP mooring site represent mean 2014–2018 velocity vectors within the OW layer (from the depth of the  $\sigma_0 = 27.80$  surface to the bottom instrument). From 2014 to 2019, RAFOS floats were tracked using an array of 13 RAFOS sound sources (circles with black cross) moored in all three sub-basins of the subpolar North Atlantic. Due to limited acoustic ranges at high latitudes, especially for floats near the sea floor, float pathways were indeterminate at the northern and southern limits of the subpolar region. The five float deployment sites are labelled as follows: EG, east Greenland; WRR, west Reykjanes Ridge; ERR, east Reykjanes Ridge; SERR, southeast Reykjanes Ridge; and CGFZ, Charlie-Gibbs Fracture Zone. Bathymetry is contoured at 1000, 2000, and 3000 m.

is the focus of this paper. To supplement the observational results, this study also uses model-simulated trajectories to provide longer and significantly more Lagrangian realizations of pathways than afforded by observations alone. In the next section, we provide background on the spread of OW in the North Atlantic. We discuss our data and methods in section 3, and then follow with results and a summary in the final two sections.

#### 2. Background

Motivated by studies in the 1990s, which suggested that the deepwater mass formed in the Labrador Sea was not confined to the Deep Western Boundary Current (DWBC) in its southward transit to the subtropical gyre (Lavender et al., 2000; Fischer and Schott, 2002), an observational study was conducted with the express purpose of tracing LSW pathways as they exited the Labrador Sea (Bower et al., 2009; Bower et al., 2011). A total of about 60 RAFOS floats were sequentially released in small groups within the DWBC near 50°N over a period of three years (Furey and Bower, 2009). While some floats did indeed make their way to the subtropical gyre within the DWBC, the majority of floats that reached the subtropical gyre did so via interior routes, rather than along the western boundary. An accompanying modeling analysis revealed this same partitioning over the temporal span that matched the observations (two years) as well as over a span of decades. A more recent observational study of LSW pathways based on 12 years of Argo float data also provides clear evidence of interior pathways for this water mass' entry into and circulation within the subtropical gyre (Biló and Johns, 2019). Collectively, these observational studies demonstrate that the DWBC is not the sole conduit for the equatorward transport. Indeed, equatorward interior pathways appear abundant in the North Atlantic.

With the recognition that the theoretical study that led to the expectation of poleward interior flow was devised to explain the circulation of *abyssal* waters, a modeling study tested whether the OW pathways exiting the Labrador Sea were any different from the observed and modeled LSW pathways (Lozier et al., 2013). In brief, while the simulated OW fluid parcels showed a greater proclivity to transit southward via the DWBC than the simulated and observed LSW, interior routes were still prevalent. In other words, even for these deepest waters of the AMOC lower limb, their equatorward spread was not confined to the DWBC.

Absent from these studies, however, was a depiction of the OW pathways within the subpolar gyre. As noted in the recent review (Bower et al., 2019), tracking the pathways of ISOW and DSOW following their entry into the North Atlantic via sills in the Greenland-Scotland Ridge is limited due to the technical challenge of float operations in descending plumes (Prater and Rossby, 2005). Our understanding of OW pathways farther downstream from the sills, where the water masses asymptote to their neutrally-buoyant depths, is better developed, but almost entirely inferred (rather than directly observed) from hydrographic property distributions and boundary current velocities. OW pathways deduced from these historical measurements have generally been depicted as confined to a deep boundary current flowing cyclonically around the three sub-basins of the subpolar region, namely the Iceland, Irminger, and Labrador basins (Fig. 1), before continuing equatorward (Bower et al., 2019). However, as with the prior view that subpolar to subtropical deepwater pathways were confined to the DWBC, there is evidence suggesting that this view within the subpolar North Atlantic is overly simplistic.

Past studies have hinted at the existence of interior OW pathways in the subpolar North Atlantic. For example, an analysis of hydrographic observations was used to suggest that not all of the relatively high-salinity ISOW flowing westward through the Charlie-Gibbs Fracture Zone (CGFZ) turns northward to continue cyclonically around the perimeter of the Irminger Basin (Stramma et al., 2004). The authors suggest that some ISOW spreads westward from the CGFZ toward Cape

Farewell and the western boundary. A similar westward (i.e., interior) ISOW pathway leading from the CGFZ was found in a study using a high-resolution ocean general circulation model (Xu et al., 2010), and recently Racapé et al (2019) described a deep Argo float trajectory as evidence of this pathway. Adding further counterevidence to the idea that OW is confined to the cyclonic boundary currents, another study used simulated trajectories and current meter data to reveal a dominant southward pathway of ISOW along the eastern flank of the Mid-Atlantic Ridge (Zou et al., 2017), consistent with tracer distributions in the area (Fleischmann et al., 2001). Finally, chlorofluorocarbon measurements in the subpolar region (LeBel et al., 2008; Smethie and Fine, 2001) show that the densest DSOW is directed offshore away from the western boundary and into the interior at the Tail of the Grand Banks.

The above-mentioned studies mainly relied on hydrographic, tracer and/or current meter data to infer pathways, and/or on simulated pathways in numerical models. An analysis of a small subset of the OSNAP floats (21 of 135) that were deployed within or traveled through the CGFZ confirmed the westward spreading of ISOW toward the Labrador basin, but also revealed a southward pathway along the western flank of the Mid-Atlantic Ridge (Zou et al., 2020). Interestingly, these floats do not show a clear or consistent northward pathway into the Irminger Sea. Thus, observational and modeling studies to date suggest that ISOW exiting westward through CGFZ is not confined to a cyclonically-flowing boundary current.

The study of DSOW pathways in the subpolar North Atlantic has received less attention. Furthermore, its study has not necessarily been distinct from studies viewing OW collectively, particularly in the Irminger and Labrador basins. For example, a question about OW pathways in these basins has been motivated by Eulerian studies of boundary current transports. Specifically, Holliday et al. (2009) noted an apparent 30% reduction in OW transport from east to west around the southern tip of Greenland. This reduction in OW led the authors to infer that some OW may flow into the interior Irminger Sea at this topographic break point. At lower latitudes, such deep boundary flow separation, either due to eddy spin-off or recirculations adjacent to the western boundary, has previously been observed (Leaman and Vertes, 1996; Bower and Hunt, 2000a; Bower and Hunt, 2000b; Bower et al., 2009; Bower et al., 2013). More recently, Pacini et al. (2020) reported a mean transport of 8.8 Sv in the OW layer west of Greenland from the first two years of OSNAP mooring data, which is  $\sim 20\%$  smaller than the mean OW layer transport east of Greenland (10.8 Sv) obtained by Hopkins et al. (2019), also using the first two years of OSNAP mooring data. Thus, the expectation that all OW rounds Cape Farewell and enters the Labrador Sea is likely not warranted.

In summary, open questions remain regarding OW pathways in the subpolar North Atlantic in large part due to the lack of direct observations of those pathways. Filling that gap to answer those questions is the focus of this paper. Specifically, we construct the large-scale spreading pathways of DSOW and ISOW downstream of their entry into the subpolar North Atlantic using a new comprehensive observational Lagrangian dataset and simulated trajectories from two models. We also study NEADW pathways from OSNAP float release sites in the Irminger basin and compare trajectories from these and all release sites.

#### 3. Data and methods

# 3.1. OSNAP float data

A total of 135 isobaric RAFOS floats (Rossby et al., 1986) were deployed at depths between 1800 and 2800 dbar along five transects across the deep boundary currents of the subpolar North Atlantic (Fig. 2). Specifically, floats were released in the deep boundary currents east of the Greenland coast (EG), within the CGFZ and west, southeast, and east of the Reykjanes Ridge (WRR, SERR and ERR, respectively). The OSNAP floats recorded daily pressure and temperature, and their positions were fixed once per day to provide eddy-resolving trajectories.

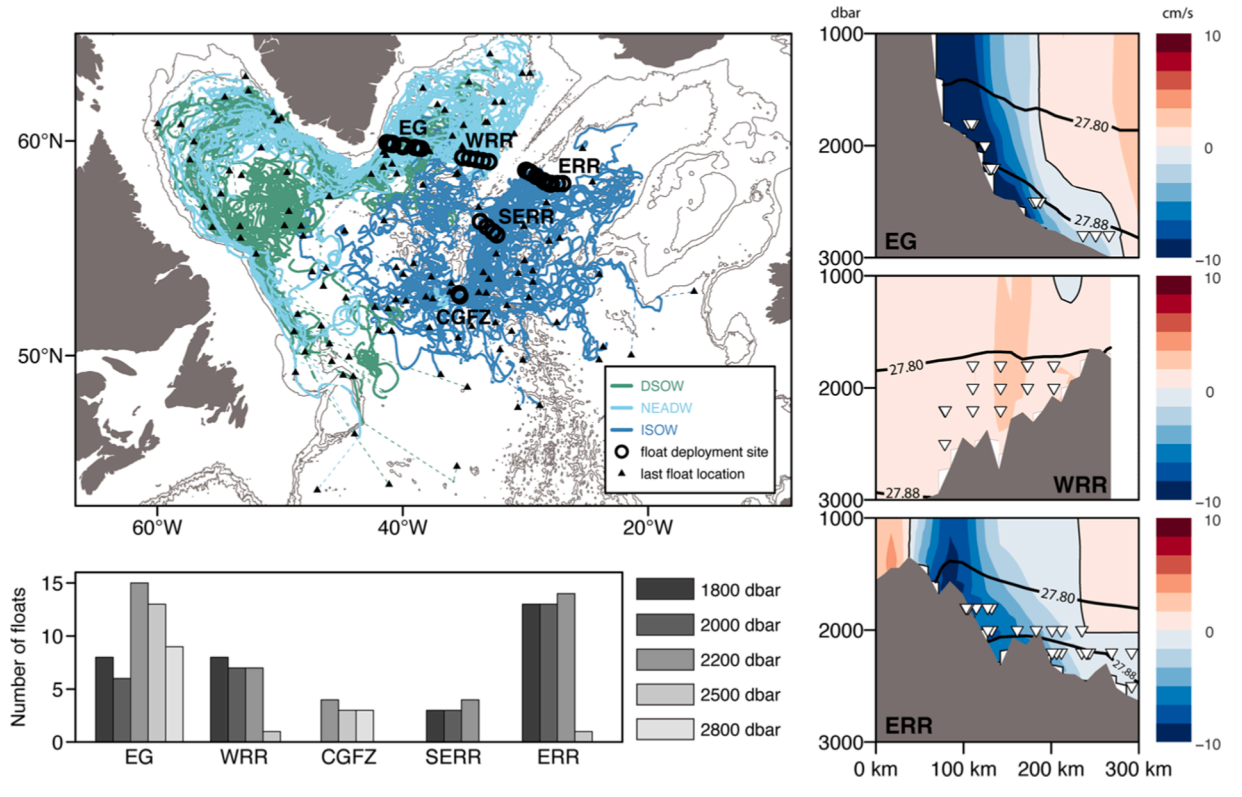


Fig. 2. Overview of all OSNAP float trajectories (top left) from the five launch sites. Trajectories are color coded to show floats embedded at launch in ISOW at ERR, SERR and CGFZ (dark blue); NEADW at WRR and EG (light blue); and DSOW at EG (dark green). Circles mark launch locations, triangles mark surface locations at floats' mission end, and dashed lines connect trajectory segments where acoustic tracking was not possible. Bathymetry is contoured at 1000, 2000, and 3000 m. (bottom left) Number of floats deployed at each site, shaded by target pressure. (right) Cross-sections of mean 2014–2018 velocity at the main float deployment locations: EG, WRR, and ERR. Along-stream velocity is shaded with 0 cm/s rendered as a thin solid black line. Thick black lines demarcate ISOW and NEADW (27.80  $\leq \sigma_0 < 27.88$ ) and DSOW ( $\sigma_0 \geq 27.88$ ). Float locations for all deployments (2014, 2015, and 2016) are marked as triangles.

At all release sites, floats were deployed in waters with density between  $\sigma_{\theta}$  = 27.80–27.88 and at all sites except CGFZ this was determined from simultaneous CTD casts. In the single CGFZ deployment, the initial position within this density layer was confirmed based on the mean hydrographic structure derived from historical data (Zou et al., 2020). While we are aware that some past studies label all water in this density range as ISOW, we restrict our labeling of ISOW to the ERR, SERR and CGFZ sites because our focus here is on tracing water mass pathways from near their entry into the subpolar North Atlantic. We label the waters in this same density class ( $\sigma_{\theta} = 27.80 - 27.88$ ) at the WRR and EG sites as NEADW. At the EG site, floats were also released in the DSOW layer, defined as waters with density exceeding  $\sigma_{\theta} = 27.88$ , and determined by simultaneous CTD casts. Thus, we assume that we are sampling ISOW pathways from ERR, SERR and CGFZ; NEADW pathways from WRR and EG; and DSOW pathways from EG. As a reminder, our use of the term 'OW' refers collectively to ISOW, DSOW and NEADW.

Most of the floats (125 of 135) were released in the summers of 2014, 2015, and 2016 for two-year missions on various OSNAP cruises and tracked using an array of RAFOS sound sources (Fig. 1). Float deployment locations were primarily at ERR, WRR and EG, along the section referred to as OSNAP East (Lozier et al., 2017). Of the 135 floats

deployed, 125 surfaced and returned data and 117 completed full programmed missions. 238 float-years of data were collected as part of this program. Further details about the float field program and data retrieval can be found in Ramsey et al. (2020).

Finally, we note that the defining isopycnals that we have used for our study can vary in depth by several hundred meters throughout the subpolar region and across the subpolar-subtropical gyre boundary (e.g., see Lozier et al., 2019; see also Fig. 2). However, we expect that the constant-pressure RAFOS float trajectories are representative of the isopycnal spreading pathways of ISOW, NEADW and DSOW due to the relative lack of velocity shear in the deep subpolar North Atlantic (e.g., Li et al., 2021).

#### 3.2. Markov chain simulations of float trajectories

To maximize the information we can extract from our Lagrangian data, we construct a Markov chain from the OSNAP float trajectories following the methods outlined in past work (Maximenko et al., 2012; Froyland et al., 2014; Miron et al., 2017; McAdam and Sebille, 2018; Drouin and Lozier, 2019; Miron et al., 2022). In brief, using a spatial resolution of 1° and a time step of 10 days, we use OSNAP float data to construct a transition matrix that details the probability of a float moving from one grid to the next within the chosen time step. We use this matrix to artificially advect particles in our domain based on these probabilities. We release particles from the three main OSNAP float deployment sites (EG, WRR, and ERR) and track them for a period of two years. Note that limited observational data precludes us from differentiating between DSOW and NEADW pathways at the EG site. Hence, the pathways produced by the Markov chain reflect pathways for all EG releases, as will be discussed further in section 4. Please see

<sup>&</sup>lt;sup>1</sup> Note that at the ERR deployment site, some of the deeper floats were seeded in densities slightly greater than 27.88  $\sigma_{\theta}$ . However, as seen from Fig. 2, all floats were in southward-moving water at launch, and most (all but one) of these floats were in the main plume of salty ISOW transported by the deep boundary current (Lozier et al. 2018; Li et al. 2021). These trajectories, as a group, do not show a systematic difference in behavior from those in the ISOW density class launched at this site (Ramsey et al. 2020). Therefore, we consider that these floats depict ISOW pathways.

Supplementary Information for details on these simulations.

## 3.3. Simulated OW pathways within ocean circulation models

To further complement the RAFOS float data, which is limited by the two-year lifetime of the floats, we simulate trajectories from the three main OSNAP deployment sites using two eddy-resolving ocean general circulation models, HYCOM and FLAME, both of which have been used extensively to study the deep North Atlantic circulation.

The HYCOM simulation we use for this study has been shown to well represent the time-mean volume transports for LSW, ISOW, and DSOW (Xu et al., 2013). This simulation also reproduces the westward ISOW transport through key locations such as the CGFZ (Xu et al., 2018). Though FLAME is no longer a widely-used model, it has been shown to nicely reproduce the transport and spreading pathways of ISOW revealed by float and mooring observations (Zou et al., 2017; Zou et al., 2020). It also compares well with tracer and float observations of LSW export pathways from the subpolar to the subtropical regions (Bower et al., 2009; Gary et al., 2012). Thus, while our primary analysis relies on HYCOM, we include FLAME in our study because of its extensive validation with observations in the deep North Atlantic, and, as will be shown, it adds considerable validity to the HYCOM results.

For both models, particles were released every 90 days in the OW layers for fifteen years at EG (NEADW and DSOW), ERR (ISOW) and WRR (NEADW). Ten-year simulated trajectories were computed by forward integrating the two-dimensional along-isopycnal velocity field in HYCOM and the three-dimensional velocity in FLAME. Please see Supplementary Information for detailed model descriptions and the definition of OW in each model.

#### 4. Results

#### 4.1. Observational pathways from the RAFOS floats

The trajectories of all OSNAP floats (Fig. 2) yield a view in sharp contrast to the expectation that OW spreading pathways are mainly confined to boundary currents, yet very much aligned with the earlier view gleaned from observed LSW pathways. Here, we also see trajectories of floats initially and intentionally deployed in boundary currents 'fill' the interiors of the Iceland, Irminger and Labrador basins over the subsequent two years from their launch (Fig. 2). While there are differences in these trajectories depending on deployment site, which we explore below, it is important to stress that not only are these pathways not confined to the boundaries, there is no evidence of a broad-scale pattern of poleward interior flow, an expectation already largely abandoned for the deep waters in the subtropical basin (Bower et al., 2019).

The large majority of the OSNAP floats remain within the subpolar region during their lifetime. Some never leave their basin of origin within two years. There are, however, some floats that make headway to the subtropics: 15 (12%) are south of 50°N at the end of their mission and 3 (2%) are south of 45°N. Since there is not a single latitude that marks the entry into the subtropics, and because the boundary between the subpolar and subtropical gyres is highly dynamic, we are left concluding that  $\sim 1\text{--}10\%$  of OSNAP floats likely entered subtropical waters near the end of their two-year mission (Fig. 2). All of the exported floats originated from either the ERR or EG deployment sites. The routes they took to the subtropics will be discussed as we next examine the pathways from each deployment site.

#### 4.1.1. Float pathways from the east Greenland (EG) site

Thirty-six floats from three different deployments at depths between 1800 and 2800 dbar at the EG site completed their two-year mission and returned good data. We begin with a discussion of the collective behavior of the EG floats, and then note differences between those launched in NEADW and those launched in DSOW. At this site, the mean along-stream velocity (Figs. 1 and 2) is strongly southward, though the

velocity considerably weakens with distance offshore.

Following their deployment, most of these 36 EG floats move swiftly to the southwest, toward the Eirik Ridge (Fig. 1), though a few (4/36 or 11%) are detrained into the Irminger Basin interior and end their mission north of the launch site (Fig. 2). All but two of the 32 floats that reach Eirik Ridge round the corner and continue to the northwest in the Labrador Sea, generally following the boundary current (Fig. S2). The fact that 30/32 (94%) of these floats round the sharply-curved Eirik Ridge and enter the Labrador Sea stands in contrast to float behavior at other sharply curved topographic features, where frequent occurrences of boundary current separation and/or eddy generation have been observed (D'Asaro, 1988; Leaman and Vertes, 1996; Bower et al., 1997; Bower et al., 2013; Solodoch et al., 2020).

Of the 30 floats that round Eirik Ridge, two do so after a 12 to 18-month circuit of the recirculation gyre east of Greenland; the rest take direct routes to the Labrador Sea. Thus, 28 of the 36 full-mission floats (78%) that were launched at the EG site stay in the deep boundary current as it transits from east to west Greenland around Eirik Ridge. The fraction of floats that did not follow this continuous route (8/36 or 22%) is remarkably similar to the difference in the transport at the OSNAP arrays mentioned above (20%; Hopkins et al., 2019; Pacini et al., 2020). While the float numbers are too few to validate the quantitative assessment of the transport difference provided by the mooring arrays, the floats do demonstrate recirculation pathways in the Irminger Sea and departures from the boundary current at the Eirik Ridge that can help explain the observed boundary current transport decrease from the east to the west side of Greenland.

Within the Labrador Sea, some EG floats follow the swift boundary current rimming the basin (Fig. 1; Zou et al., 2021), while others deflect into the interior along the west coast of Greenland or as they travel southeastward along the Labrador coast (Fig. 2). Most floats that exit the Labrador Sea do so via the deep western boundary current, though some offshore detrainment occurs at Orphan Knoll and the Flemish Cap. From their launch at EG, the swiftest floats reach the vicinity of the Flemish Cap in approximately two years.

Possible NEADW and DSOW pathway differences are noted along the Labrador coast at Hamilton Bank, at  $\sim55^{\circ}\text{N}$ , where some floats are diverted into the interior once they encounter an outcrop (or 'spur') along the relatively smooth slope. Of the 21 floats that travel in the boundary current along this western slope, 5/21 (24%) are diverted into the interior Labrador Sea at this location (Fig. 2, also Fig. S1), with floats embedded in DSOW twice as likely (3/9 or 33%) than those embedded in NEADW (2/13 or 15%) to be diverted. Because this difference is based on small numbers and because the general behavior of NEADW pathways is similar to DSOW pathways, a result confirmed with our model simulations, for the remainder of the paper we proceed with the understanding that a description of the observational EG pathways pertains to both NEADW and DSOW. However, we will distinguish these water masses in our model simulations.

# 4.1.2. Float pathways from the west Reykjanes Ridge (WRR) site

Twenty-two floats from two different deployments at the WRR site, launched between 1800 and 2500 dbar, returned good data. As seen in Figs. 1 and 2, the mean along-stream velocity at this location is weakly northward, but only for a narrow core centered around 150 km (Fig. 2). Outside of this core, and particularly further offshore, the mean velocity is negligible. However, as has recently been described (de Jong et al., 2020), the along-boundary velocity here is highly variable, so much so that it is at times southward. The impact of this weak northward mean flow is evident in the slow northward progress of the WRR floats following their launch (Figs. 2 and S1). That northward progress is characterized by substantial deflection into the basin interior, leading to just a handful of floats that loosely follow the isobaths to the northern part of the basin.

Those WRR floats that find their way to the western boundary of the basin are entrained into the swift deep boundary current east of Greenland (Figs. 1 and 2) and then quickly dispatched to the Labrador Sea. There are two fates for the WRR floats: either they remain in the Irminger Sea (9/22 or 41%) or they end up in the Labrador Sea at the completion of their mission west of 45°W (13/22 or 59%). Not surprisingly, floats in the latter group exhibit behavior similar to the EG floats after they reach the western boundary of the Irminger Sea.

#### 4.1.3. Float pathways from the Charlie-Gibbs Fracture Zone (CGFZ) site

Nine float trajectories from a single deployment at the CGFZ site in 2015, launched between 1800 and 2800 dbar, have previously been described (Zou et al., 2020), so here we give just a brief summary. This float deployment site is not on the OSNAP line, so there is no contemporaneous background velocity and density field at the time of deployment. However, earlier moored arrays (Saunders, 1994; Bower and Furey, 2017) measured westward mean flow at the depths and launch positions of the floats. OSNAP floats launched at this site move swiftly westward and subsequently either turn southward along the Mid-Atlantic Ridge or west-northwestward toward the Labrador Sea.

# 4.1.4. Float pathways from the east Reykjanes Ridge (ERR) and the southeast Reykjanes Ridge (SERR) sites

Thirty-eight RAFOS floats released between 1800 and 2500 dbar at the ERR site over three years (2014, 2015 and 2016) returned good data. The mean along-stream velocity where the floats were launched is southwestward, with magnitude decreasing with distance from the Reykjanes Ridge crest (Figs. 1 and 2). From their launch location, most floats (32/38; 84%) roughly follow the isobaths for their first  $\sim 100$ days, but then the most inshore floats tend to move westward into the Irminger Sea via gaps in the Reykjanes Ridge. [The westward passage of shallow ISOW through gaps in the Reykjanes Ridge has been previously described by McCartney, 1992; Xu et al., 2010; Zou et al., 2017; and Petit et al., 2018.] In particular, 7/38 (18%) ERR floats cross the Reykjanes Ridge upstream of the CGFZ (Fig. S3); approximately half through the Bight Fracture Zone (BFZ) at 57°N and half through the 'noname' fracture zone region at about 55.5°N. These seven ERR floats were all ballasted for 1800 dbar, such that 7/13 or just over half the shallowest floats left the Iceland Basin through gaps in the ridge before reaching the CGFZ. We attribute this leakage to the fact that the 1800 dbar floats were released closer to the ridge crest-launched on the western end of the ERR line-and that they were shallow enough to cross the ridge through these gaps. The sill depth of the BFZ, for example, is  $\sim 2000\ \text{m}.$  The remaining 31 floats travel past the entrance to the BFZ and other gaps in the ridge and continue moving southward to the CGFZ region at ~ 52.5°N. From there, 11 floats move westward (consistent with Racapé et al., 2019) and an equal number move to the northeast, back into the Iceland Basin (Figs. 2 and S2). The end-positions of those floats that travel westward through the CGFZ are mainly along the western Mid-Atlantic Ridge or at the southern extent of the Labrador Sea. As noted earlier (e.g., Daniault et al., 2016; Zou et al., 2017; Petit et al., 2022), it appears that the ERR floats that arrive in the Irminger Sea do so via the gaps mentioned above, rather than via a boundary current flowing from the CGFZ northward into the Irminger Sea (Fig. S3).

Ten RAFOS floats released between 1800 and 2500 dbar at the SERR site during the summer of 2017 returned good data. The behavior of these floats is similar to the behavior of the ERR floats (Fig. S1), as this site is just  $\sim 400~\rm km$  downstream of the ERR site. From this launch site, 2/10 (20%) floats crossed the ridge near or through the 'no-name' gap. Like the ERR floats that escaped to the Irminger Basin through gaps in the ridge (Fig. S3), these two floats were launched at 1800 dbar. Interestingly, even with the small number of floats deployed at the SERR site, all of the same fates observed for the ERR floats in the southern Iceland Basin are manifest here. This distribution hints at the presence of robust mean pathways, which will be explored in the following sections.

#### 4.2. Simulated pathways from a Markov chain

Utilizing a Markov chain simulation described in section 3, we recreate particle pathways from our three main deployment sites, EG, WRR, and ERR (Fig. 3, top panels). Launch locations for these simulated trajectories match the deployment sites of the OSNAP floats shown in Fig. 2. For the reason discussed above, we are not distinguishing between floats launched in DSOW and those launched in NEADW. The reader is reminded that though this Markov chain simulation yields the envelope of possible trajectories from each launch site, there is no temporal variability associated with these trajectories. Thus, the distributions in Fig. 3 show a time-invariant view of the particles for the years 2014–2018. Finally, we note that our construction of the Markov chain is limited to north of 50°N due to sparse observational data south of that latitude (Fig. 2).

EG simulations reveal the quick export of particles from the Irminger Sea. After two years, most particles released at the EG site are in the Labrador Sea, where they have almost equal representation in the interior and in the boundary currents. We note that these simulations reveal the 2-year advective time scale noted earlier for the transit of the EG particles to the exit of the Labrador Sea. The swift export of these EG particles is attributed to the strong boundary currents off the east Greenland coast and on both sides of the Labrador Sea (Fig. 1).

The simulations from the WRR site reveal slower spreading from the release site. After two years, particles are still likely to be in the Irminger Sea, though the boundary current in the Labrador Sea off the west coast of Greenland is also a likely end position for these simulated particles. The spatial distribution of these WRR-launched particles in the Labrador Sea is similar to that for the EG-launched particles (though the probabilities are overall weaker), indicating that the pathways for these WRR particles mimic those for EG once they are in the boundary current off of east Greenland.

After initiation at the ERR site, the large majority of particles remain in the Iceland Basin after two years. However, several pathways leading out of this basin are highly probable. One of those pathways leads into the Irminger Sea via gaps in the Reykjanes Ridge. The northward extension of this pathway, along the cyclonic boundary current of the Irminger Sea, is noted by the high probability along the western flank of the ridge. Particles taking this route can reach the eastern boundary of the Labrador Sea after two years, though the likelihood of this end position is an order of magnitude smaller than an end position within the Iceland Basin. Two other pathways are evident in these plots: a westward pathway through the CGFZ (and subsequent spreading to the south and west) and a more diffuse spreading to the southeast, on the eastern side of the Mid-Atlantic Ridge. Importantly, the 'traditional' ISOW pathway (Fig. 1) does not emerge as a strong contender from this analysis, namely there is very little probability of an ISOW pathway that passes through the CGFZ and then on into the Irminger Sea via a cyclonic boundary current. Instead, the ERR particles in the Irminger Sea at the end of two years have largely entered the basin through the gaps north of the CGFZ.

A comparison of the spread from the EG and ERR sites reveals a major difference between these two sites. EG particles are quickly exported from the Irminger Sea and are essentially 'on their way' to the subtropical region after only two years, having rapidly circuited the Labrador Sea with the help of the strong, deep boundary currents in that basin. In contrast, ERR particles advect more slowly out of the Iceland Basin along several spreading pathways, only one of which is associated with a deep boundary current. The southward spread of these water masses is also differentiated by their probability east of the Mid-Atlantic Ridge: the EG-launched particles have a negligible presence in this region. Finally, we note that the Markov chain pathways described here agree with the pathways described by Miron et al. (2022) using transition path theory.

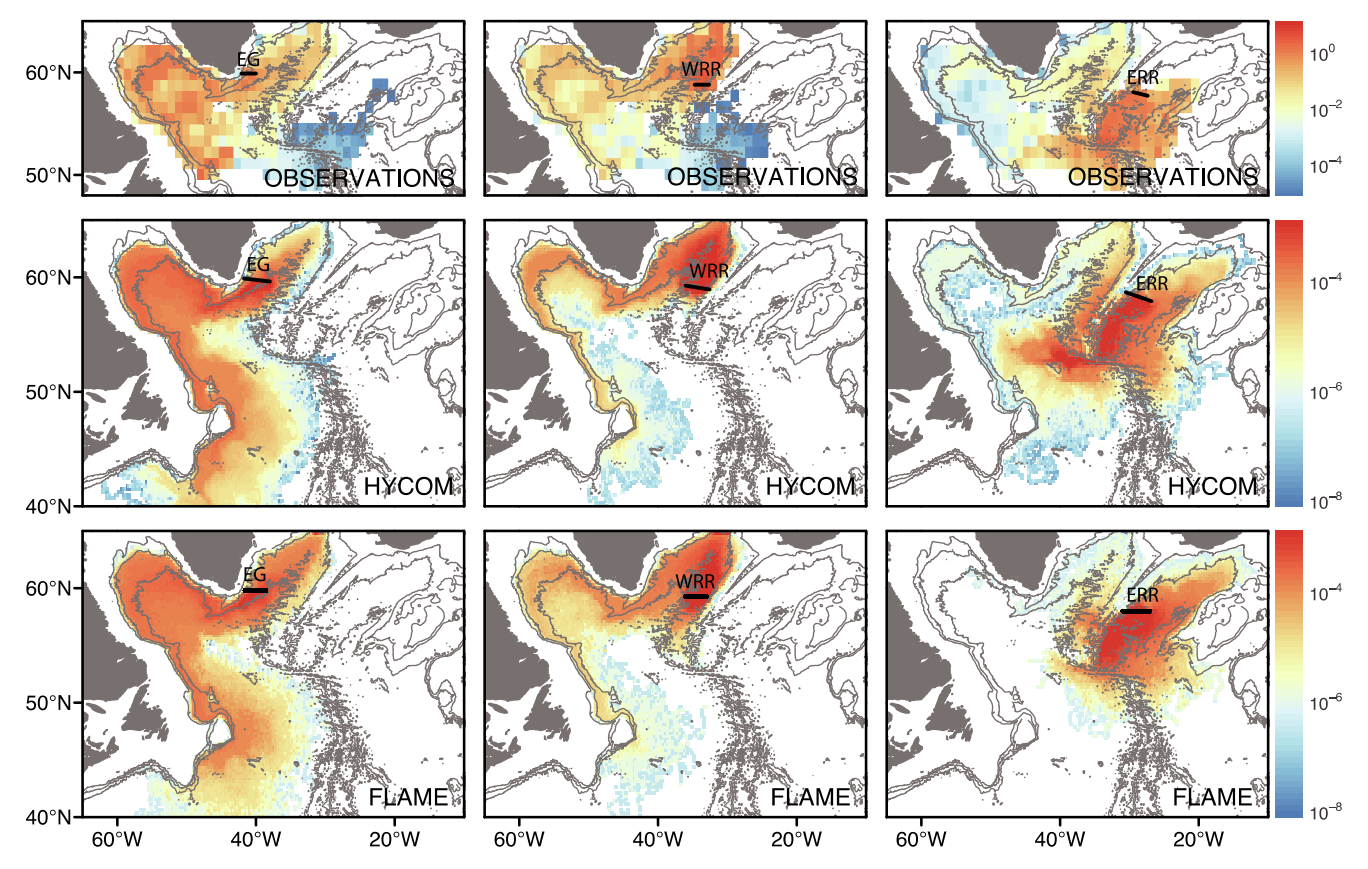


Fig. 3. Cumulative two-year probability distributions from the Markov chain (top panels), HYCOM (middle panels) and FLAME (bottom panels) simulations. Particles were released at the EG (left panels), WRR (middle panels) and ERR (right panels) sites in the subpolar North Atlantic. The probability distribution is shown as the percentage of particle positions such that the total value of all grid cells adds up to 100%. 200000, 200000, and 300,000 particles are launched from the EG, WRR, and ERR deployment sites, respectively, for the Markov chain. 11,820 (5940 in NEADW and 5880 in DSOW), 4320 (in NEADW), and 6600 (in ISOW) particles are launched from the EG, WRR, and ERR deployment sites, respectively, for HYCOM. 6236 (4670 in NEADW and 1566 in DSOW), 7286 (in NEADW) and 6236 (in ISOW) particles are launched from the EG, WRR, and ERR deployment sites, respectively, for FLAME. At each grid point, the particle count is inclusive of all layers defined as OW (see Supplementary Information). Bathymetry is contoured at 1000, 2000, and 3000 m.

## 4.3. Simulated pathways from numerical models

Mimicking the OSNAP deployments, particles are initialized in both models within the ISOW layer at ERR, the NEADW layer at WRR and within both NEADW and DSOW at the EG site, and then tracked for two years using model velocity fields (Fig. 3, middle and bottom panels). The simulated particle trajectories, ranging from 4,000–11,000 depending on launch site, far outnumber the OSNAP float trajectories.

The probability distribution of the EG particles (inclusive of NEADW and DSOW) is remarkably similar in these two models (Fig. 3, middle and bottom panels) and compares favorably with the spread inferred from the OSNAP float Markov chain (Fig. 3, top panels). Particles quickly exit the Irminger Sea, and travel within the boundary current into and around the Labrador Sea. As with the OSNAP float trajectories, the simulated trajectories reveal strong, though not complete, continuity around Eirik Ridge. The particles fill the interior of the Labrador Sea and exit that basin primarily along the western boundary. The two-year distributions, restricted to the western basin of the North Atlantic, spread into the subtropics to  $\sim 40^{\circ}N$  for both models. There are, of course, some differences to note in these distributions—for example, HYCOM has higher probabilities in the boundary currents than FLAME (especially south of Flemish Cap) and, conversely, lower probabilities in the interior-but they are slight. We consider this model-model similarity remarkable. A separation of the EG particles into those released in the NEADW density range from those released in the DSOW range reveals for both models (Fig. S4) the slightly greater likelihood for the DSOW particles to be detrained into the interior compared to NEADW

particles, as will be discussed further in section 4.4. Finally, it is important to note that these modeling simulations, which extend to  $40^{\circ}N$ , reveal the entry of the simulated particles into the subtropical gyre, whereas the Markov chain simulation, limited to north of  $50^{\circ}N$ , does not. However, we note that a few observational float trajectories continue their journey southward beyond  $50^{\circ}N$ , providing evidence for southward penetration in the western basin (Figs. 2 and S1) within two years.

Model simulations of water mass spreading from the WRR site are also remarkably similar to each other and to the Markov chain distribution, as they both indicate a strong accumulation of particles within the Irminger Sea and a rapid transit into the Labrador Sea once particles are entrained into the boundary current off east Greenland. As these particles sweep around the rim of the Labrador Sea, they also penetrate the interior, though the probability of finding WRR particles in the interior of the Labrador Sea after two years is relatively low.

Finally, the models' spreading patterns from the ERR site are broadly similar, though not as favorable as for the other two sites. As with the OSNAP trajectories, these simulated trajectories reveal strong retention within the Iceland Basin, as well as southward movement along the eastern flank of the Mid-Atlantic Ridge via the southward boundary current (Figs. 1 and 2). Also, in agreement with observations, both simulated distributions show 1) leakage of ISOW water across the gaps north of the CGFZ and into the Irminger Sea, 2) southward spreading of ISOW into the West European Basin, and 3) westward spreading from the CGFZ. The main difference between these distributions is that HYCOM has a much faster spread than FLAME. In effect, it looks as

though the FLAME particles are headed to all the same places that the HYCOM particles are, yet their travel time is longer, as next examined.

A quantification of the transit times of OW from one basin to the next facilitates a validation of the model simulations with observations and brings the difference among the three release sites into sharper focus. For this quantification, the subpolar North Atlantic is divided into five regions: Labrador Sea, Irminger Sea, Iceland Basin, a region to the east of the CGFZ and south of the Iceland Basin, and a region to the west of the CGFZ and south of the Irminger and Labrador Basins (Fig. 4). Once particles are released from the three deployment sites (EG, WRR and ERR), their positions within each of these regions are tracked over two years to produce, for each launch site: a) the percent of the total launched particles that reside within each region at a particular point in time (line plots in Fig. 4) and b) the cumulative percentage of total launched particles that have visited each region by a particular point in time (shading in Fig. 4). The values indicated by the line plots sum to 100% at each point in time, while the values indicated by the shading do not. If, for example, all launched particles visited not only their launch region, but also another region, the shading for each of those regions would indicate 100%.

The temporal and spatial distribution of the model simulated

particles from the EG site match remarkably well with the distribution of the Markov chain (Fig. 4, left panels). As time progresses, the Irminger Sea loses particles to the Labrador Sea, which then loses them to the West CGFZ. After two years, it is apparent that almost all EG-launched particles visited the Labrador Sea and about 50% entered the West CGFZ. The simulated distributions from WRR show a similar match with the observations-based Markov chain (Fig. 4, middle panels). The contrast of note is not that between the simulated and observed trajectories, but rather the differences between the two release sites. The takeaway here is that a majority of the waters flowing through the WRR site are still within the Irminger Sea after two years, in sharp contrast to the waters flowing through the EG site. About 25% of particles released from the WRR site have visited the Labrador Sea after two years, and even less (~5%) have visited the west CGFZ region.

As expected from the probability maps discussed previously, differences between the observed and simulated distributions show up at the ERR site (Fig. 4, right panels). Interestingly, in most cases the model simulations bracket the observed behavior. Departures out of the Iceland Basin are fast (slow) relative to the observations in HYCOM (FLAME); more (fewer) particles than observed enter West CGFZ for HYCOM (FLAME); and more (fewer) particles than observed enter the Irminger

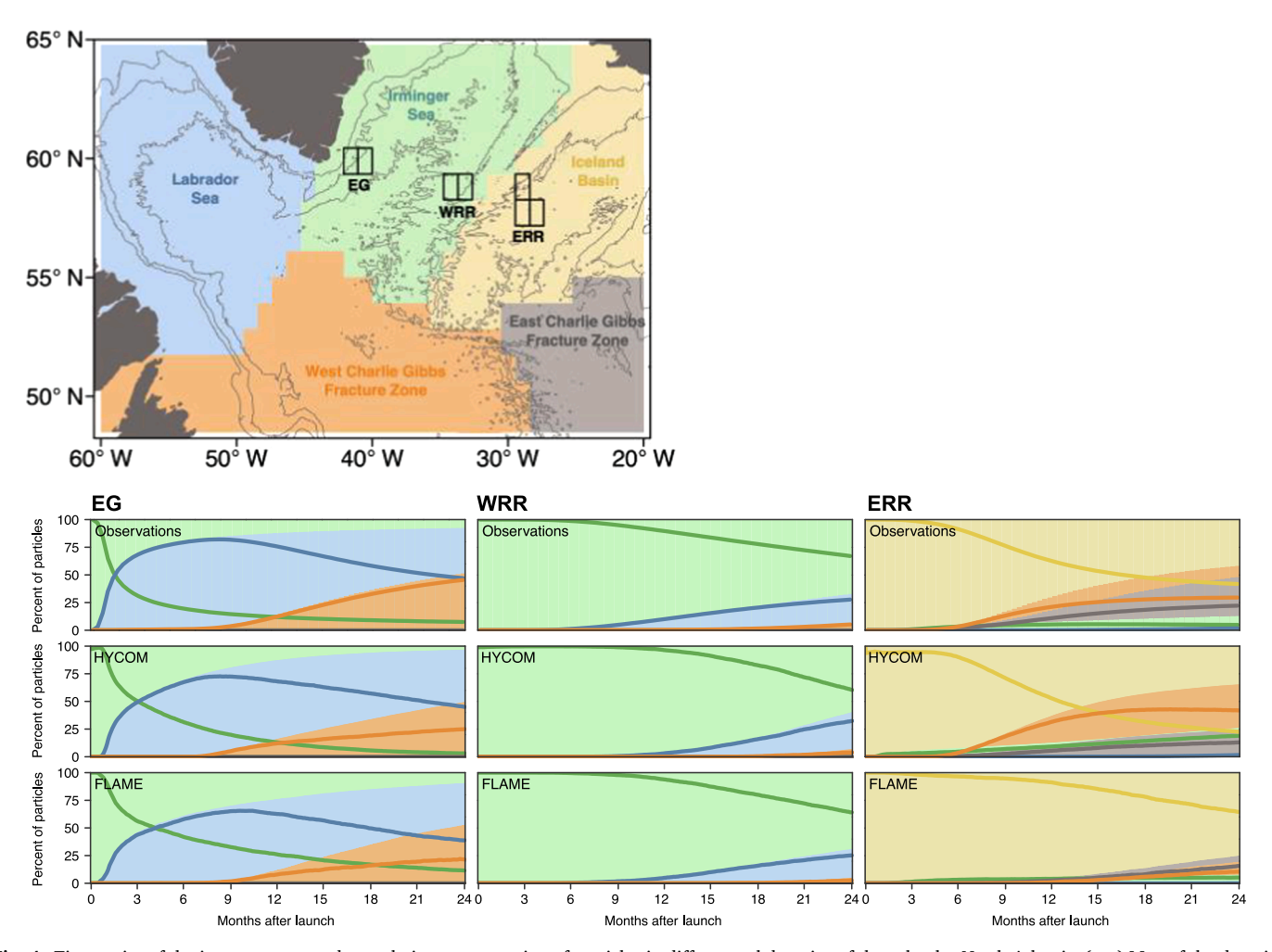


Fig. 4. Time series of the instantaneous and cumulative concentration of particles in different subdomains of the subpolar North Atlantic. (top) Map of the domain with five subdomains: Blue = Labrador Sea; green = Irminger Sea; yellow = Iceland Basin; gray = east of the Charlie Gibbs Fracture Zone; orange = west of the Charlie Gibbs Fracture Zone. The three different release sites are shown by black grid boxes. Bathymetry is contoured at 1000, 2000, and 3000 m. (bottom) Nine panels are organized by model: top row, Markov chain; middle, HYCOM; bottom, FLAME; and by release site: left column, EG; middle, WRR; and right, ERR. For all panels, shaded regions show cumulative percentage of particles that have visited a particular subdomain by a particular time. A value of 100% means that all particles visited that subdomain. Note that the shading overlaps. For example, in the upper left panel, all particles (100%) were released in the Irminger Sea (green shading) and this percentage does not change over time. However, the lower portion of the green shaded region is covered as particles enter other regions. Lines show percentage of particles present in a particular subdomain at a specific point in time.

Sea for HYCOM (FLAME). However, both simulations show less penetration into East CGFZ than observed from the Markov chain. This may be because 5 of the 6 floats that made it into East CGFZ were from the SERR deployment, and model particles were initialized at the ERR site only. After two years, about 50% of the particles based on the observations have visited the west CGFZ region (60% HYCOM, 20% FLAME), and 40% have visited the east CGFZ (10% HYCOM, 20% FLAME). Visits to Irminger Basin are less than 10% in the observations and in FLAME, but about 15% in HYCOM.

These simulations have revealed that HYCOM hews more faithfully to the observations for some metrics and FLAME for others. However, there are far more agreements than disagreements in all of these comparisons, leading us to conclude that the generalizations regarding the spread of OW from EG and ERR drawn from the limited OSNAP observations are robust.

In summary, the main result from these simulations is the difference between the spread of water from the ERR site (ISOW) and that from the EG site (NEADW and DSOW). The latter largely conforms to the long-standing expectation that OW pathways are mostly contained within the boundary current as they transit the subpolar North Atlantic, yet the former stands in stark contrast to that expectation.

#### 4.4. Long-term fate of OW in the North Atlantic

With confidence in the model simulations of the observed spreading patterns, the strong similarity in the model simulations, and an understanding that the differences in OW spreading patterns are primarily expressed from launches at the EG and ERR sites, we focus our investigation on the long-term fate of OW in the North Atlantic with ten-year HYCOM simulations at these two sites (FLAME simulations are shown in Fig. S5). Here, however, we distinguish between NEADW and DSOW at the EG site as we are particularly interested in the long-term fate of DSOW in comparison to that of ISOW, as revealed from the ERR launch, and the model simulations allow for that distinction. We include the NEADW launch at EG for completeness and to compare its spreading

pathway to ISOW (which shares its density) and to DSOW (which shares its launch location).

The penetration of both DSOW and NEADW from the EG site into the subtropical region (Fig. 5, top left and center panels) is reminiscent of the previously studied OW pathways from the exit of the Labrador Sea that showed interior as well as boundary pathways in numerical simulations (Lozier et al., 2013). The spread from the EG site for both water masses is mostly similar, as they are both largely confined to the west of the Mid-Atlantic Ridge, but that confinement is complete for DSOW. Furthermore, while both water masses reach  $\sim 20^{\circ} N$  over the ten years of integration, NEADW shows a greater eastward spread as these water masses penetrate to that latitude. In contrast, the spread of particles from the ERR site (ISOW) ten years after launch (Fig. 5, top right panel) highlights the importance of the southward pathway into the West European Basin (see Xu et al., 2010; Zou et al., 2017; Xu et al., 2018 for further discussion). The westward spreading through the CGFZ is also highlighted in this simulation.

The differences between the OW pathways entering the subtropical region from the EG and ERR sites is further illustrated by the distribution of particles that reach 45°N within ten years (Fig. 5, bottom panels). Clearly, the DSOW and NEADW pathways from the EG site are largely restricted to the west of the Mid-Atlantic Ridge, while ISOW spreading from the ERR site straddles both sides of this ridge. While illustrative, we note here that only 79.9% (38.9%) of the total particles launched at EG (ERR) have reached this latitude after ten years. As such, we expect a broad age distribution for the OW waters that enter the subtropical region regardless of origin.

To quantify pathway preference over a ten-year span, we calculate the percentage of particles that spread southward through the DWBC, those that take interior pathways to the west of the Mid-Atlantic Ridge and those that take interior pathways to the east of this ridge; see Supplementary Table S1. For those particles launched at EG, the DWBC is the dominant pathway at 50°N, yet the interior pathway to the west of the Mid-Atlantic Ridge is more predominant by 45°N, and by 40°N this interior pathway accounts for more than 85% of the particles that reach

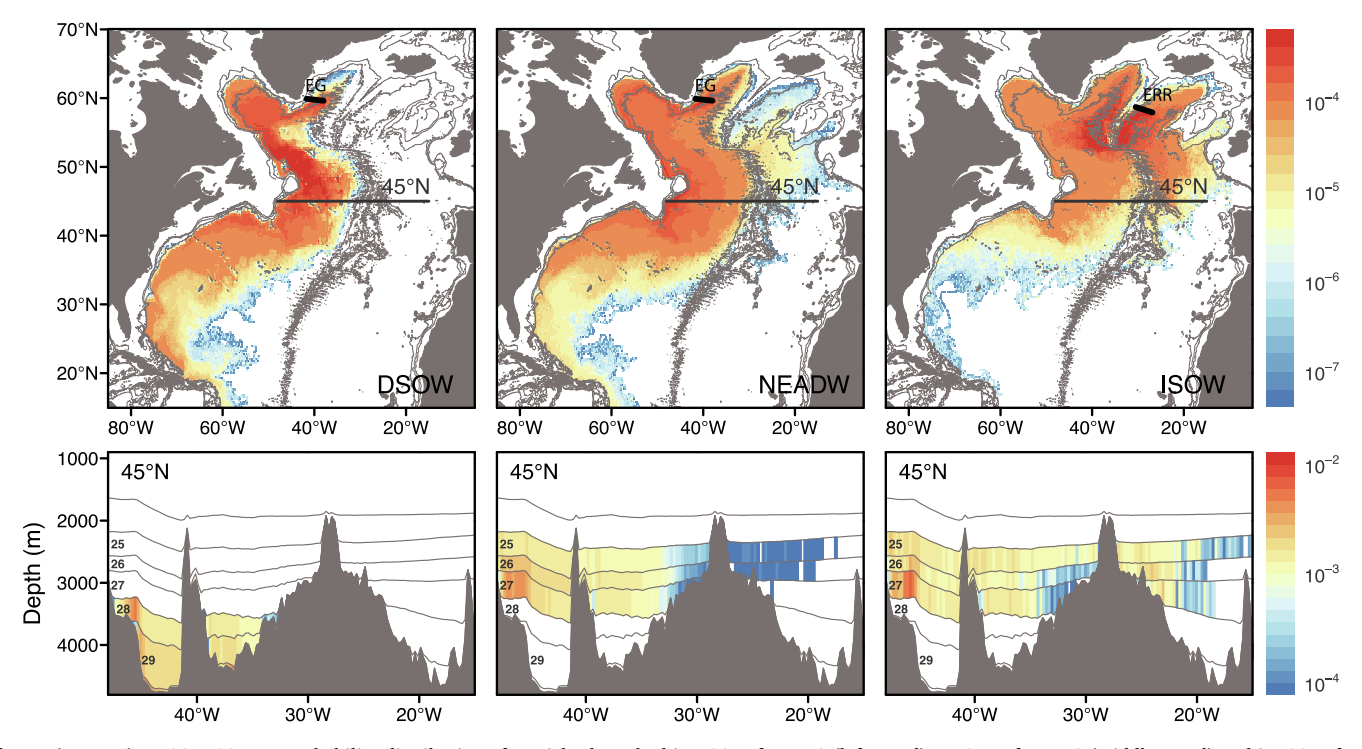


Fig. 5. (top row) HYCOM 10-year probability distribution of particles launched in DSOW from EG (left panel), NEADW from EG (middle panel) and in ISOW from ERR (right panel). Launch locations, indicated as black lines, are the same as in Fig. 3, as are the particle numbers. Bathymetry is contoured at 1000, 2000, and 3000 m. (bottom row) Probability distribution of particles across  $45^{\circ}$ N launched from EG in DSOW and NEADW (left and middle panels, respectively) and ERR (right panel). Black lines show the time-averaged model isopycnic coordinate (in  $\sigma_2$ ). Numbers indicate HYCOM layers, as defined in the main text.

this latitude. For the ERR releases, the DWBC still dominates at  $50^{\circ}N$  for HYCOM, but only marginally. At  $45^{\circ}N$  and  $40^{\circ}N$ , the interior pathway west of the ridge is preferred. Consistent with our previous model comparisons, FLAME shows a preference for interior pathways at all three latitudes:  $50^{\circ}N$ ,  $45^{\circ}N$  and  $40^{\circ}N$ . We note that the total fraction of ERR-released particles that reach  $40^{\circ}N$  in 10 years is only 15.8% in HYCOM and 3.5% in FLAME, indicating that most OW particles take more than 10 years to reach  $40^{\circ}N$ . As such, our simulations do not identify preferred pathways on longer time scales.

Finally, we note here that in the absence of an observational float program purposely designed to study the subpolar-subtropical Lagrangian connection (the OSNAP float program was principally constructed to study OW pathways in the subpolar region), we are relying on these model simulations to infer the subpolar-subtropical gyres connection. However, the connection revealed by these simulations is broadly consistent with current meter data that reveals a southward ISOW pathway along the eastern flank of the Mid-Atlantic Ridge (Zou et al., 2017), tracer distributions mentioned earlier (Fleischmann et al., 2001; LeBel et al., 2008; Smethie and Fine, 2001) and the penetration of DSOW into the subtropics as revealed by chlorofluorocarbons (Rhein et al., 2015).

Lacking ten-year observed pathways, we compare the distributions in Fig. 5 with a cross-section of climatological mean salinity at 45°N (Fig. 6). We first note the strong (fresh) influence of DSOW to the west of the Mid-Atlantic Ridge, beneath the 27.88 isopycnal (Fig. 6). Below the salty thermocline waters of the North Atlantic Current and the fresh LSW that extends to approximately 2000 m, relatively high salinity waters stretch across the entire basin between the 27.80 and 27.88 isopycnals. The salinities in this density range (occupied by ISOW and NEADW in the subpolar North Atlantic) east of the Mid-Atlantic Ridge are much higher than those to the west, perhaps reflecting the fact that these waters are bracketed by the relatively fresh LSW (above) and DSOW (below) in the western basin. We note though that LSW lies above waters in this density range in the eastern basin as well. The cross-basin difference in salinity might also be attributed to the simple fact that the transit time for ISOW (with a stronger salinity signature than NEADW) to reach the eastern basin is shorter than its transit time to the western basin since diffusion and mixing affect the salinity signature over different path lengths.

Finally, we note that both water masses appear to be broadly distributed in this climatological salinity section: over the western basin for DSOW, and over the entire width of the Atlantic for ISOW/NEADW. Synoptic sections obviously reveal more spatial variability. For example,

a 1982 hydrographic section across 47°N has a salinity signature of ISOW/NEADW flowing down both sides of the Mid-Atlantic Ridge, but no such salinity signature is evident along the western boundary (McCartney, 1992). Similar results can be found along the WOCE AR19 repeat line (Lumpkin et al., 2008).

#### 4.5. Origin of the NEADW in the Irminger basin

Since the observed and simulated spreading of ISOW from ERR give little indication of a direct and coherent pathway for this water mass into the Irminger basin, we turn next to an investigation of the origin of NEADW that resides in the Irminger basin. This analysis is also motivated by the clear salinity distinction seen in Fig. 6 between the waters east and west of the Mid-Atlantic Ridge in this density range.

We use model output to initialize backward-trajectories from the EG and WRR sites within the NEADW density range. The trajectories are integrated backward in time for ten years to identify the sources for the waters that find their way to these sites in that time frame. We are specifically interested in understanding the prevalence of waters from the ERR site (where we have ISOW) that source the EG and WRR sites. The distributions from the backward trajectories (Fig. 7) reveal that the EG site is sourced with waters over a broad swath of the western subpolar region. Consistent with the distributions from the forward integrations, the Iceland basin is shown to be among those sources. However, this region is a weak contributor in both models: within ten years, only 17% of the waters at the EG site can be traced to the Iceland Basin for HYCOM and only 6% for FLAME (Fig. 7, bottom panel).

Repeating this exercise for the WRR site reveals similar results, though here the Iceland Basin is a larger contributor, as expected due to its proximity to WRR (Fig. 7). In fact, 42% of the waters at the WRR site can be traced to the Iceland Basin within ten years for HYCOM, and 30% for FLAME (Fig. 7, bottom panel). The difference is consistent with the fact that there is a stronger ISOW transport in HYCOM (than in FLAME) into the Irminger Sea (e.g., Zou et al., 2017; Xu et al., 2018). Collectively, the spreading pattern for the simulated forward and backward trajectories, as well as the OSNAP floats, suggest that NEADW at the EG site is likely a mixture of 1) relatively young ISOW that has reached the Irminger Sea via gaps along the Reykjanes Ridge, 2) older ISOW that has recirculated within the subpolar North Atlantic and 3) a mixture of ISOW, DSOW and LSW that has resulted from diapycnal mixing in the basin, as revealed recently by oxygen measurements along a Deep-Argo float trajectory (Racapé et al., 2019).

These Lagrangian analyses lend credence to the characterization of

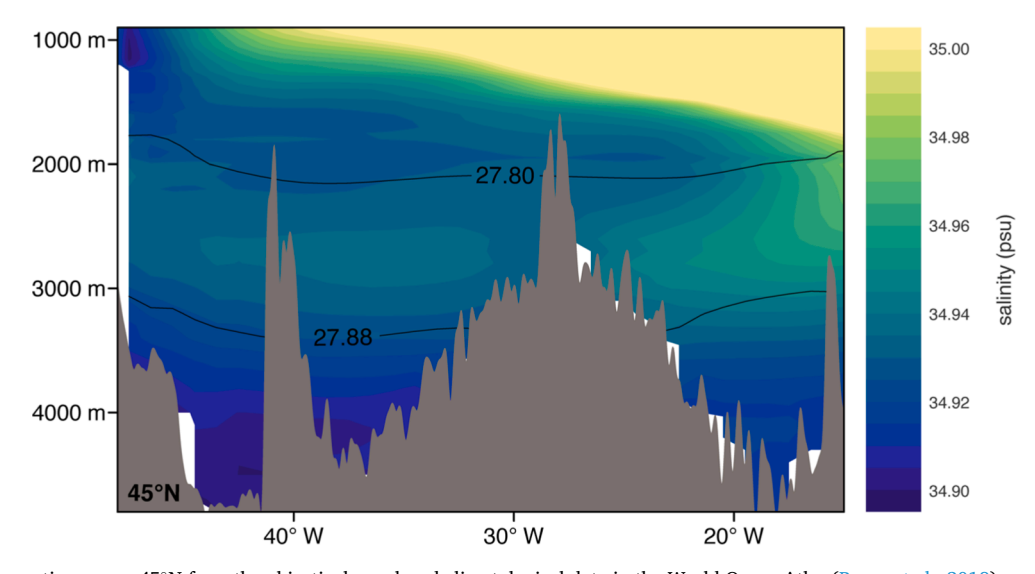


Fig. 6. Mean salinity section across 45°N from the objectively analyzed climatological data in the World Ocean Atlas (Boyer et al., 2018).  $\sigma_{\theta}$  contours of 27.80 and 27.88 are drawn as solid black lines.

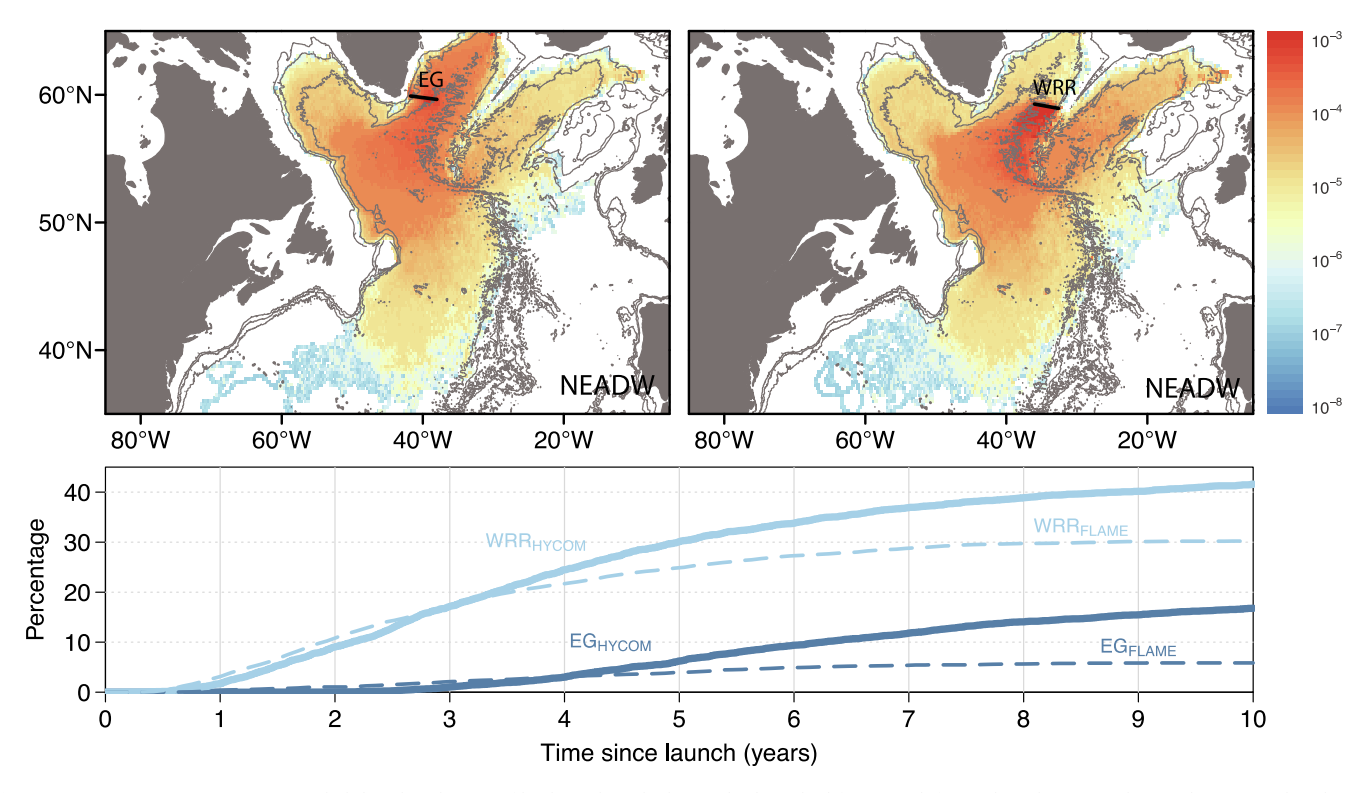


Fig. 7. (top row) Ten-year HYCOM probability distribution of backward-tracked particles launched from EG (left panel) and WRR (right panel); FLAME distribution is not shown. Particles are launched in the NEADW layer at both sites. Distributions are computed from 5940 particles for the EG release and 4140 particles for the WRR release. Bathymetry is contoured at 1000, 2000, and 3000 m. (bottom) The percentage of particles backtracked into the Iceland Basin (at the ERR site) as a function of time for both release sites and for both HYCOM and FLAME. Lines are labelled to indicate model and release site.

water in the ISOW density range within the Irminger as NEADW (Swift, 1984; Dickson et al., 1994; Lazier et al., 2002) rather than ISOW and they help to explain the cross Mid-Atlantic Ridge difference in salinity at 45°N. Specifically, the salinity to the east of the Mid-Atlantic Ridge is likely a signature of the younger (i.e., saltier ISOW) that has taken a fairly direct route to that latitude, whereas the salinity to the west of the Mid-Atlantic Ridge likely reflects older ISOW (i.e., less salty) because of its longer transit time since entry into the North Atlantic and the accompanying mixing during that time.

#### 5. Summary

The central question regarding spreading pathways of the deep North Atlantic waters over the past two decades has been a relatively simple one, namely are they restricted to the boundary currents? Though the question itself is simple, its answer has far-reaching implications for our theoretical understanding of the deep velocity fields in the North Atlantic and for our understanding of the linkage between water mass variability and AMOC variability. Accordingly, we first summarize our answer to the question and then discuss these implications.

From this study's comprehensive view of OW spreading pathways in the subpolar North Atlantic based on direct measurements, supplemented by model simulations, we can state unambiguously that deepwater pathways are not restricted to the boundary currents of the basin. In contrast to a now decades-old theory, and in support of more recent studies, these deep waters, which find their origin in the Nordic Seas, spread equatorward along several pathways, including—but certainly not restricted to—the deep western boundary currents. This analysis has revealed distinctly different spreading patterns for DSOW and ISOW.

Following its entry into the North Atlantic via the Denmark Strait, DSOW is advected along the swift deep boundary currents of the

Irminger and Labrador Seas. Though the boundary transport of this water mass is strikingly apparent, so too is the penetration of this water mass into the interior of these basins. The penetration illustrated here from float pathways is consistent with hydrographic observations along the OSNAP section (Lozier et al., 2019) that clearly show DSOW "painting" the bottom of these basins, particularly the Labrador Sea. While previous model results (Xu et al., 2015) showed the DSOW spread into the interior Labrador Sea from the Greenland side, our observational results show an unexpected DSOW penetration into the interior from the Labrador side of the basin, likely due to topographic interactions.

The ISOW spread out of the Iceland Basin sharply contrasts with the spreading pattern of DSOW. This deep-water mass filters out of the Iceland Basin more slowly and along multiple pathways. Importantly, the floats provide no evidence for what has traditionally been considered ISOW's main pathway through the subpolar North Atlantic, namely a transit along a deep boundary current that wraps cyclonically around the rims of the Iceland, Irminger and Labrador basins. Instead, ISOW export pathways out of the Iceland Basin include direct entry into the Irminger Sea through gaps in the Reykjanes Ridge north of the CGFZ; a slow, southeastward spreading toward the West European Basin; and, following transit through the CGFZ, westward spreading toward the Labrador Sea and southward spreading along the western flank of the Mid-Atlantic Ridge. In short, pathways other than the DWBC are the norm, and not the exception, for this deep-water

NEADW spreading from the Irminger basin reveals a pattern more reminiscent of DSOW spreading than ISOW spreading, a fact that highlights an obvious conclusion: a common launch location trumps a shared density class. While NEADW bears more hydrographic similarities to ISOW, once it is in the deep boundary current off east Greenland, it shares a dynamic similarity to DSOW as it transits downstream, hence a shared pattern of spreading.

Modeling simulations reveal the entry of these deep-water masses into

the North Atlantic subtropics. DSOW is restricted to the western basin as it transits southward, with a predominant, but not exclusive, presence in the deep boundary current. NEADW shares this pattern of entry, though it has some limited presence east of the Mid-Atlantic Ridge. By contrast, ISOW has a significant presence on both sides of the Mid-Atlantic Ridge and in the West European Basin as it transits southward.

The move away from a paradigm that constrains all deep-water pathways to the western boundary leaves us with the question as to the mechanisms governing the deep velocity fields in the North Atlantic. Though evident that DSOW and NEADW pathways within the Irminger and Labrador Seas are constrained by the strong and deep boundary currents of the wind-driven subpolar gyre, the mechanisms governing their export to the subtropics are unclear. Equally unclear are the mechanisms responsible for the multi-path spread of ISOW within the subpolar region and on to the subtropics. Though we understand in general that zonal and meridional density gradients likely play a role, as does potential vorticity conservation, the particular forcing that yields these spreading patterns and is responsible for their differences, is not completely understood.

We suggest though that a dominant factor in determining these differences is simply one of geography. As ISOW leaves the Iceland Basin it comes in close contact with the energetic, deep-reaching, eastwardflowing northern branch of the North Atlantic Current in the vicinity of the CGFZ (Bower and Furey, 2017; Zou et al., 2017). A prior study (Zou et al. 2020) has demonstrated how OSNAP ISOW floats exiting westward from the CGFZ appear to be influenced by the mesoscale variability of the overlying North Atlantic Current. This study surmised that ISOW is directed along various pathways according to the synoptic, timedependent position and strength of the North Atlantic Current, a situation analogous to the dynamics at the Gulf Stream-Deep Western Boundary Current cross-over near Cape Hatteras. There, DSOW along the western boundary is observed to veer offshore into deeper water to conserve potential vorticity in response to the deepening pycnocline associated with the Gulf Stream (Bower and Hunt, 2000b). The location of offshore deflection was highly variable and depended on the instantaneous position of the meandering Gulf Stream, much like what is observed for the ISOW floats as they approach, transit, and exit the CGFZ. As DSOW and NEADW circulate along the boundary currents of the Irminger and Labrador Seas, their pathways are unimpeded by the North Atlantic Current. Instead, their pathways are largely determined by the deep-reaching cyclonic wind-driven gyre in the subpolar region. Their entry into the subtropics and their subsequent southward transit along the DWBC and interior pathways, however, are likely impacted by eddy-driven recirculations driven by the energetic Gulf Stream and North Atlantic Current (Lozier 1997; Gary et al. 2011).

The move away from a paradigm that constrains all deep water to the western boundary has implications for the assumed linkage between western boundary current transport and AMOC transport, and between deep-water mass variability and AMOC variability. First, it has become increasingly clear that not all deep water in the lower AMOC limb is transported equatorward by the western boundary currents of the North Atlantic. Thus, a measure of the deep-water transport within only the boundary currents cannot be considered an assessment of the total equatorward deep-water transport.

Secondly, the assumption that variability in deep-water formation drives downstream AMOC variability has been considerably weakened by a host of studies, including this one. As evident from the spreading pathways shown here, the deep waters that are carried equatorward will have a large range in age, as measured by the elapsed time since their formation via convection. This large range is the result of myriad pathways for the deep waters to transit equatorward, including local recirculations that increase path lengths and transit times, and mixing along those pathways. Thus, interannual to decadal variability in source water formation is unlikely to be clearly or simply expressed downstream since formation anomalies do not move coherently downstream on those time scales. In other words, AMOC variability on interannual to

decadal times scales is unlikely directly linked to upstream variability in deep-water formation. Recent studies have suggested that density anomalies along the western boundary of the North Atlantic may instead be generated locally and/or remotely by wind and buoyancy forcing unrelated to deep-water formation (Zou et al., 2019; Zou et al., 2020). So, while we understand that boundary density anomalies determine AMOC variability, the source of those density anomalies is no longer assumed to be strictly tied to deep-water mass variability.

Finally, reconstructions of AMOC variability from proxy data, involving either the strength of boundary currents and/or the property variability of deep waters, will need to account for the myriad equatorward pathways of DSOW and ISOW, but particularly so for the latter.

Author Contributions.

ASB and MSL conceived and designed the OSNAP float program. ASB and HHF executed the OSNAP float field program. MSL led the analyses and writing of this study. HHF and ASB provided the analysis of the observational data, KLD provided the Markov-chain analysis, SZ and XX provided the model simulations and their analysis and KLD and HHF refined all figures. All authors contributed to the writing and editing of the manuscript.

#### **Declaration of Competing Interest**

The authors declare that they have no known competing financial interests or personal relationships that could have appeared to influence the work reported in this paper.

#### Data availability

RAFOS float data can be accessed at Woods Hole Open Access Server (https://doi.org/10.26025/1912/24388). All other data will be made available on request.

#### Acknowledgments

MSL gratefully acknowledges the support from the Physical Oceanography Program of the U.S. National Science Foundation (Grant OCE-2017522). ASB, HHF and SZ gratefully acknowledge the support from the Physical Oceanography Program of the U.S. National Science Foundation (Grant OCE-1756361). KLD gratefully acknowledges the support from the Physical Oceanography Program of the U.S. National Science Foundation (Grant OCE-1851075). XX gratefully acknowledges the support from the Physical Oceanography Program of the U.S. National Science Foundation (Grant OCE-2038449). RAFOS float data can be accessed at Woods Hole Open Access Server (https://doi.org/10.26025/1912/24388).

# Appendix A. Supplementary material

Supplementary data to this article can be found online at https://doi.org/10.1016/j.pocean.2022.102874.

#### References

Biastoch, A., Böning, C.W., Getzlaff, J., Molines, J.-M., Madec, G., 2008. Causes of interannual-decadal variability in the Meridional Overturning Circulation of the midlatitude North Atlantic Ocean. J. Clim. 21 (24), 6599–6615.

Biló, T.C., Johns, W.E., 2019. Interior pathways of Labrador Sea Water in the North Atlantic from the Argo perspective. Geophys. Res. Lett. 46 (6), 3340–3348.

Bower, A., et al., 2019. Lagrangian views of the pathways of the Atlantic Meridional Overturning Circulation. *J. Geophys.* Res. Oceans 124 (8), 5313–5335.

Bower, A., Lozier, S., Gary, S., 2011. Export of Labrador Sea Water from the subpolar North Atlantic: A Lagrangian perspective. Deep Sea Res. 2 Top. Stud. Oceanogr. 58 (17–18), 1798–1818.

Bower, A., Furey, H., 2017. Iceland- Scotland Overflow Water transport variability through the Charlie-Gibbs Fracture Zone and the impact of the North Atlantic Current. J. Geophys. Res.: Oceans 122 (9), 6989–7012.

- Bower, A.S., Hendry, R.M., Amrhein, D.E., Lilly, J.M., 2013. Direct observations of formation and propagation of subpolar eddies into the subtropical North Atlantic. Deep Sea Res. 2 Top. Stud. Oceanogr. 85, 15–41.
- Bower, A.S., Hunt, H.D., 2000a. Lagrangian Observations of the Deep Western Boundary Current in the North Atlantic Ocean.: Part I: Large-scale pathways and spreading rates. J. Phys. Oceanogr. 30 (5), 764–783.
- Bower, A.S., Hunt, H.D., 2000b. Lagrangian observations of the Deep Western Boundary Current in the North Atlantic Ocean.: Part II: The Gulf Stream-Deep Western Boundary Current crossover. J. Phys. Oceanogr. 30 (5), 784–804.
- Bower, A.S., Armi, L., Ambar, I., 1997. Lagrangian observations of meddy formation during a Mediterranean Undercurrent seeding experiment. J. Phys. Oceanogr. 27 (12), 2545–2575.
- Bower, A.S., Lozier, M.S., Gary, S.F., Böning, C.W., 2009. Interior pathways of the North Atlantic Meridional Overturning Circulation. Nature 459 (7244), 243–247.
- Boyer, Tim P.; Garcia, Hernan E.; Locarnini, Ricardo A.; Zweng, Melissa M.; Mishonov, Alexey V.; Reagan, James R.; Weathers, Katharine A.; Baranova, Olga K.; Seidov, Dan; Smolyar, Igor V. (2018). World Ocean Atlas 2018. Temperature and Salinity. NOAA National Centers for Environmental Information. Dataset. <a href="https://www.ncei.noaa.gov/archive/accession/NCEI-WOA18">https://www.ncei.noaa.gov/archive/accession/NCEI-WOA18</a>. Accessed April 27, 2022.
- Broecker, W., 1991. The great Ocean Conveyor. Oceanography 4, 79-89.
- Daniault, N., et al., 2016. The northern North Atlantic Ocean mean circulation in the early 21st century. Prog. Oceanogr. 146, 142–158.
- D'Asaro, E.A., 1988. Generation of submesoscale vortices: A new mechanism. J. Geophys. Res. Oceans 93 (C6), 6685–6693.
- de Jong, M.F., Steur, L., Fried, N., Bol, R., Kritsotalakis, S., 2020. Year-round measurements of the Irminger Current: Variability of a two-core current system observed in 2014–2016. J. Geophys. Res. Oceans 125 (10).
- Delworth, T., Manabe, S., Stouffer, R.J., 1993. Interdecadal variations of the thermohaline circulation in a coupled ocean-atmosphere model. J. Clim. 6 (11), 1993–2011.
- Desbruyères, D.G., Mercier, H., Maze, G., Daniault, N., 2019. Surface predictor of overturning circulation and heat content change in the subpolar North Atlantic. Ocean Sci. Discuss. 15 (3), 1–21.
- Dickson, R.R., Brown, J., 1994. The production of North Atlantic Deep Water: Sources, rates, and pathways. J. Geophys. Res. 99 (C6), 12319–12341.
- Doney, S.C., Jenkins, W.J., 1994. Ventilation of the Deep Western Boundary Current and abyssal western North Atlantic: Estimates from Tritium and 3He distributions. J. Phys. Oceanogr. 24 (3), 638–659.
- Drouin, K.L., Lozier, M.S., 2019. The surface pathways of the South Atlantic: Revisiting the cold and warm water routes using observational data. *J. Geophys.* Res. Oceans 124 (10), 7082–7103.
- Fischer, J., Schott, F.A., 2002. Labrador Sea Water tracked by profiling floats—From the Boundary Current into the open North Atlantic. J. Phys. Oceanogr. 32 (2), 573–584.
- Fischer, J., Visbeck, M., Zantopp, R., Nunes, N., 2010. Interannual to decadal variability of outflow from the Labrador Sea. Geophys. Res. Lett. 37 (24).
- Fleischmann, U., Hildebrandt, H., Putzka, A., Bayer, R., 2001. Transport of newly ventilated deep water from the Iceland Basin to the Westeuropean Basin. Deep Sea Res. 1 Oceanogr. Res. Pap. 48 (8), 1793–1819.
- Froyland, G., Stuart, R.M., van Sebille, E., 2014. How well-connected is the surface of the global ocean? Chaos 24 (3), 033126.
- Furey H., A. Bower, "Export pathways from the subpolar North Atlantic: DLD2 RAFOS Float Data Report July 2003–November 2008" (WHOI Tech. Rep. WHOI-2009-06, 2009).
- Gary, S.F., Lozier, M.S., Böning, C.W., Biastoch, A., 2011. Deciphering the pathways for the deep limb of the Meridional Overturning Circulation. Deep Sea Res. Part II 58 (17–18). 1781–1797.
- Gary, S.F., Lozier, M.S., Biastoch, A., Böning, C.W., 2012. Reconciling tracer and float observations of the export pathways of Labrador Sea Water. Geophys. Res. Lett. 39 (24).
- Holliday, N.P., Bacon, S., Allen, J., 2009. Circulation and transport in the western boundary currents at Cape Farewell Greenland. J. Phys. Oceanogr. 39 (8), 1854–1870.
- Hopkins, J.E., et al., 2019. Transport variability of the Irminger Sea Deep Western Boundary Current from a mooring array. J. Geophys. Res. Oceans 124 (5), 3246–3278.
- Lavender, K.L., Davis, R.E., Owens, W.B., 2000. Mid-depth recirculation observed in the interior Labrador and Irminger Seas by direct velocity measurements. Nature 407 (6800), 66–69.
- Lazier, J., Hendry, R., Clarke, A., Yashayaev, I., Rhines, P., 2002. Convection and restratification in the Labrador Sea, 1990–2000. Deep Sea Res. I Oceanogr. Res. Pap. 49 (10), 1819–1835.
- Leaman, K.D., Vertes, P.S., 1996. Topographic influences on recirculation in the Deep Western Boundary Current: Results from RAFOS float trajectories between the Blake-Bahama Outer Ridge and the San Salvador "Gate". J. Phys. Oceanogr. 26 (6), 941–961.
- Li, F., Lozier, M.S., 2018. On the Linkage between Labrador Sea Water volume and overturning circulation in the Labrador Sea: A case study on proxies. J. Clim. 31 (13), 5225–5241.
- Li, F., Lozier, M.S., Holliday, N.P., Johns, W.E., Le Bras, I.A., Moat, B.I., de Jong, M.F., 2021. Observation-based estimates of heat and freshwater exchanges from the subtropical North Atlantic to the Arctic. Prog. Oceanogr. 197, 102640.
- Lozier, M.S., 1997. Evidence for large-scale eddy-driven gyres in the North Atlantic. Science 277 (5324), 361–364.
- Lozier, M.S., 1999. The impact of mid-depth recirculations on the distribution of tracers in the North Atlantic. Geophys. Res. Lett. 26 (2), 219–222.

- Lozier, M.S., et al., 2017. Overturning in the Subpolar North Atlantic Program: A new international ocean observing system. Bull. Am. Meteorol. Soc. 98 (4), 737–752.
- Lozier, M.S., et al., 2019. A sea change in our view of overturning in the subpolar North Atlantic. Science 363, 516–521.
- LeBel, D.A., et al., 2008. The formation rate of North Atlantic Deep Water and Eighteen Degree Water calculated from CFC-11 inventories observed during WOCE. Deep Sea Res. 1 Oceanogr. Res. Pap 55 (8), 891–910.
- Lozier, M.S., Gary, S.F., Bower, A.S., 2013. Simulated pathways of the Overflow Waters in the North Atlantic: Subpolar to subtropical export. Deep Sea Res. 2 Top. Stud. Oceanogr. 85, 147–153.
- Lumpkin, R., Speer, K.G., Koltermann, K.P., 2008. Transport across 48°N in the Atlantic Ocean. J. Phys. Oceanogr. 38 (4), 733–752.
- Maximenko, N., Hafner, J., Niiler, P., 2012. Pathways of marine debris derived from trajectories of Lagrangian drifters. Mar. Pollut. Bull. 65 (1–3), 51–62.
- McAdam, R., van Sebille, E., 2018. Surface connectivity and interocean exchanges from drifter-based transition matrices. J. Geophys. Res. Oceans 123 (1), 514–532.
- McCartney, M.S., 1992. Recirculating components to the deep boundary current of the northern North Atlantic. Prog. Oceanogr. 29 (4), 283–383.
- Miron, P., et al., 2017. Lagrangian dynamical geography of the Gulf of Mexico. Sci. Rep. 7 (1), 1-12.
- Miron, P., Beron-Vera, F.J., Olascoaga, M.J., 2022. Transition paths of North Atlantic Deep Water. J. Atmos. Oceanic Technol.
- Pacini, A., et al., 2020. Mean conditions and seasonality of the West Greenland Boundary Current System near Cape Farewell. J. Phys. Oceanogr. 50 (10), 2849–2871.
- Petit, T., Mercier, H., Thierry, V., 2018. First direct estimates of volume and water mass transports across the Reykjanes Ridge. *J. Geophys.* Res. Oceans 123 (9), 6703–6719.
- Petit, T., Thierry, V., Mercier, H., 2022. Deep through-flow in the Bight Fracture Zone and its imprint in the Irminger Sea. EGUsphere [preprint]. https://doi.org/10.5194/ egusphere-2022-248.
- Pickart, R.S., 1992. Water mass components of the North Atlantic Deep Western Boundary Current. Deep Sea Res. A 39 (9), 1553–1572.
- Polo, I., Robson, J., Sutton, R., Balmaseda, M.A., 2014. The importance of wind and buoyancy forcing for the boundary density variations and the geostrophic component of the AMOC at 26° N. J. Phys. Oceanogr. 44 (9), 2387–2408.
- Prater, M.D., Rossby, T., 2005. Observations of the Faroe Bank Channel overflow using bottom-following RAFOS floats. Deep Sea Res. 2 Top. Stud. Oceanogr. 52 (3–4), 481–494.
- Racapé, V., Thierry, V., Mercier, H., Cabanes, C., 2019. ISOW spreading and mixing as revealed by Deep-Argo floats launched in the Charlie-Gibbs fracture zone. J. Geophys. Res. Oceans 124 (10), 6787–6808.
- Ramsey, A.L., Furey, H.H., Bower, A.S., 2020. Overturning of the Subpolar North Atlantic Program (OSNAP): RAFOS Float Data Report June 2014 January 2019. Rhein, M., Kieke, D., Steinfeldt, R., 2015. Advection of North Atlantic Deep Water from
- Rhein, M., Kieke, D., Steinfeldt, R., 2015. Advection of North Atlantic Deep Water from the Labrador Sea to the southern hemisphere. J. Geophys. Res. Oceans 120 (4), 2471–2487.
- Richardson, P.L., 2008. On the history of meridional overturning circulation schematic diagrams. Prog. Oceanogr. 76, 466–486.
- Rossby, T., Dorson, D., Fontaine, J., 1986. The RAFOS System. J. Atmos. Ocean. Technol. 3 (4), 672–679.
- Saunders, P.M., 1994. The flux of overflow water through the Charlie-Gibbs Fracture Zone. J. Geophys. Res. 99 (C6), 12343–12355.
- Smethie Jr, W.M., Fine, R.A., Putzka, A., Jones, E.P., 2000. Tracing the flow of North Atlantic Deep Water using chlorofluorocarbons. J. Geophys. Res. 105 (C6), 14297–14323.
- Solodoch, A., McWilliams, J.C., Stewart, A.L., Gula, J., Renault, L., 2020. Why odes the Deep Western Boundary Current "leak" around Flemish Cap? J. Phys. Oceanogr. 50 (7), 1989–2016.
- Srokosz, M., Danabasoglu, G., Patterson, M., 2021. Atlantic Meridional Overturning circulation: Reviews of observational and modeling advances—An introduction. J. Geophys. Res. Oceans 126 (1).
- Stommel, H., 1958. The abyssal circulation. Deep Sea Res. 5, 80–82.
- Stommel, H., Arons, A.B., 1959. On the abyssal circulation of the world ocean—I. Stationary planetary flow patterns on a sphere. Deep Sea Res. 1953 (6), 140–154.
- Smethie Jr., W.M., Fine, R.A., 2001. Rates of North Atlantic Deep Water formation from chlorofluorocarbon. Deep Sea Res. 1 Oceanogr. Res. Pap. 48 (1), 189–215.
- Stramma L., D. Kieke, M. Rhein, F. Schott, I. Yashayaev, K. P. Koltermann, Deep water changes at the western boundary of the subpolar North Atlantic during 1996 to 2001. Deep Sea Res. 1 Oceanogr. Res. Pap., 51(8), 1033–1056 (2004).
- Swift, J.H., 1984. The circulation of the Denmark Strait and Iceland-Scotland Overflow Waters in the North Atlantic. Deep Sea Res. A 31 (11), 1339–1355.
- Toole, J.M., Andres, M., Le Bras, I.A., Joyce, T.M., McCartney, M.S., 2017. Moored observations of the Deep Western Boundary Current in the NW Atlantic: 2004–2014. J. Geophys. Res.: Oceans 122 (9), 7488–7505.
- Warren, B.A., 1981. Deep circulation of the world ocean. Evolution of Physical Oceanography 6–41.
- Wunsch, C., 2005. The total meridional heat flux and its oceanic and atmospheric partition. J. Clim. 18 (21), 4374–4380.
- Xu, X., et al., 2013. On the currents and transports connected with the Atlantic meridional overturning circulation in the subpolar North Atlantic. *J. Geophys.* Res. Oceans 118 (1), 502–516.
- Xu, X., Schmitz Jr, W.J., Hurlburt, H.E., Hogan, P.J., Chassignet, E.P., 2010. Transport of Nordic Seas Overflow Water into and within the Irminger Sea: An eddy-resolving simulation and observations. J. Geophys. Res. 115 (C12).
- Xu, X., Rhines, P.B., Chassignet, E.P., Schmitz Jr., W.J., 2015. Spreading of Denmark Strait overflow water in the western subpolar North Atlantic: Insights from eddyresolving simulations with a passive tracer. J. Phys. Oceanogr. 45 (12), 2913–2932.

- Xu, X., Bower, A., Furey, H., Chassignet, E.P., 2018. Variability of the Iceland-Scotland Overflow Water transport through the Charlie-Gibbs Fracture Zone: Results from an eddying simulation and observations. J. Geophys. Res. Oceans 123 (8), 5808–5823.
- Yeager, S., Danabasoglu, G., 2014. The origins of late-twentieth-century variations in the large-scale North Atlantic circulation. J. Clim. 27 (9), 3222–3247.
- Zhang, R., 2010. Latitudinal dependence of Atlantic Meridional Overturning Circulation (AMOC) variations. Geophys. Res. Lett. 37 (16).
- Zou, S., et al., 2021. Observed deep cyclonic eddies around Southern Greenland. J. Phys. Oceanogr. 51 (10), 3235–3252.
- Zou, S., Lozier, S., Zenk, W., Bower, A., Johns, W., 2017. Observed and modeled pathways of the Iceland Scotland Overflow Water in the eastern North Atlantic. Prog. Oceanogr. 159, 211–222.
- Zou, S., Lozier, M.S., Buckley, M., 2019. How is meridional coherence maintained in the lower limb of the Atlantic Meridional Overturning Circulation? Geophys. Res. Lett. 46 (1), 244–252.
- Zou, S., Bower, A., Furey, H., Susan Lozier, M., Xu, X., 2020. Redrawing the Iceland-Scotland Overflow Water pathways in the North Atlantic. Nat. Commun. 11 (1), 1–8.